PAPER

Check for updates

Alkylation of α-pinene with isobutene/isobutane over Hβ zeolite†

Zhaocai Jiao,‡ Mingzu Liu,‡ Ningbo Yang, Fengli Yu, [ID] Congxia Xie, [ID] Shitao Yu and Bing Yuan [ID] *

α-Pinene and isobutene/isobutane can undergo hybrid alkylation under acid catalysis, resulting in C_{14} and C_{20} product fractions with favorable bio-based high-energy-density fuel properties after hydrogenation. In this study, the catalytic performance of zeolite molecular sieves, such as Hβ, HY, HZSM-5, HZSM-35, HSAPO-11, was investigated for the alkylation of α-pinene and Isobut-5 (a mixture of isobutene/isobutane with a mass ratio of 1:5) given the acidic sites and specific pore structures with shape-selective abilities of zeolite catalysts. Various characterization techniques, including temperature-programmed desorption of ammonia (NH_3-TPD), Fourier transform infrared spectroscopy with pyridine adsorption (Py-IR), N_2 adsorption/desorption, X-ray fluorescence spectrum (XRF), and particle size analysis, were conducted to analyze the acidic properties, pore characteristics, silica−aluminum ratio, and grain size of the zeolites, and their influence on the alkylation of α-pinene and Isobut-5. Moreover, the recycling performance of the favorite Hβ-25n catalyst and an effective regeneration method were investigated using temperature-programmed oxidation (TPO) analysis. This study provides essential research data for the preparation of α-pinene-based high-energy-density fuels.

Introduction

Due to concerns regarding resource depletion, carbon emissions, and air pollution resulting from fossil fuels, the development of alternative fuels derived from biomass platform compounds has emerged as a promising direction in recent years.[1,2] While significant signs of progress have been made in the production of biofuels as replacements for gasoline[3,4] and diesel,[5,6] research on bio-based high-energy-density fuels (Bio-HEDF) primarily used in air vehicles and airborne missiles with superior volumetric calorific value and low-temperature mobility[7] has lagged. On the other hand, the preparation of biofuels derived from platform compounds sourced from lignocellulose, the most abundant form of biomass in nature, faces challenges in terms of harsh hydrodeoxygenation conditions[8,9] and low atomic utilization[10,11] due to the high oxygen content in the feedstock's structure. However, thanks to its naturally oxygen-free rigid polycyclic structure, α-pinene, the principal constituent of turpentine, has gained attention in recent years as a promising feedstock with high atom economy for developing advanced rocket fuels with enhanced density

and combustion properties.[12,13] Furthermore, although the current yield of α-pinene from turpentine is insufficient to meet the demand for biofuels, metabolic engineering, and synthetic biology approaches offer avenues for creating novel and cost-effective pathways for the biosynthesis of these monoterpenes.[14,15]

However, the density and calorific value of saturated alkanes obtained from the hydrogenation of C_{10} polycyclic terpenes, such as α-pinene, are not satisfactory, particularly due to their high flash point, which prevents their direct use as HEDF.[16] Therefore, carbon-increasing reactions need to be employed to enhance their properties, including density, calorific value, viscosity, and flash point. Among these reactions, the acid-catalyzed dimerization of pinene has been found to produce C_{20} dimers with excellent density and calorific value, but poor low-temperature performance due to their high viscosities and freezing points.[17] Alternatively, carbon-increasing products with favorable fuel properties can also be obtained through the cyclopropanation of pinene.[18] However, the preparation process involved the use of organic solvents, a non-recyclable Zn carbene catalyst, and a diiododimethane carbon-increasing module, resulting in poor atom economy.

In our research, we have discovered that blended isobutene/isobutane, a low-cost feedstock for alkylated gasoline, can undergo cross-alkylation with α-pinene.[19,20] The resulting C_{14} hydrocarbons, obtained after hydrogenating the alkylation products, exhibited favorable properties such as high calorific

State Key Laboratory Base of Eco-chemical Engineering, College of Chemistry and Molecular Engineering, College of Chemical Engineering, Qingdao University of Science and Technology, Qingdao, 266042, China. E-mail: yuanbing@qust.edu.cn

† Electronic supplementary information (ESI) available. See DOI: https://doi.org/10.1039/d4ya00291a
‡ The two authors have the same contribution to this study.

value and low viscosity. As a result, this method is anticipated to be an effective approach for upgrading biomass resources and obtaining high-energy-density fuels. Previous studies have revealed that, under the catalysis of phosphotungstic acid (HPW), the reaction system involving α-pinene and isobutane/isobutene is prone to undergo α-pinene isomerization,[21] α-pinene dimerization,[13] and even trimerization, as well as self-alkylation of C_4 mixed hydrocarbons,[22] in addition to cross-alkylation to produce C_{14} hydrocarbons. However, the density and volumetric heat value of the self-alkylation products from C_4 hydrocarbons are far from meeting the requirements of aviation fuels.[20] Additionally, the presence of α-pinene oligomers, which are difficult to be removed by distillation, will damage the cryogenic properties of the resultant mixed fuel. Therefore, this study aims to investigate the effects of acid sites distribution,[23] pore structure,[24] and particle size[25,26] of various molecular sieves, namely Hβ, HY, HZSM-5, HZSM-35, and HSAPO-11, on the catalytic performance and product distribution of α-pinene alkylation with isobutene/isobutane. The objective of this research is to provide fundamental research data for the controlled preparation of α-pinene-based high-energy-density hybrid fuels and explore efficient processing routes.

Experimental

Chemicals and materials

ZSM-5 (SiO_2/Al_2O_3 = 25, Na_2O < 0.1 wt%), Y (SiO_2/Al_2O_3 = 5, Na_2O < 0.3 wt%), ZSM-35 (SiO_2/Al_2O_3 = 25, Na_2O < 0.1 wt%), and SAPO-11 (SiO_2/Al_2O_3 = 0.5, Na_2O < 0.1 wt%) zeolites were purchased from Nankai Catalysts Company, China. β-25n (nano-sized, SiO_2/Al_2O_3 = 25, Na_2O < 0.07 wt%) was provided by the laboratory of Dalian University of Technology. β-25m (micron-sized, SiO_2/Al_2O_3, Na_2O < 0.1 wt%) and β-50m (micron-sized, SiO_2/Al_2O_3 = 50, Na_2O < 0.03 wt%) were purchased from Shandong Hefa Environmental Protection Technology Co., Ltd. Phosphotungstic acid ($H_3PW_{12}O_{40}\cdot xH_2O$, 99%) was obtained from Shanghai Aladdin Biochemical Technology Co., Ltd. α-Pinene (98 wt%) was purchased from Jiangxi Hexin Chemical Co., Ltd. A mixed isobutene/isobutane feedstock (with a mass ratio of 1:5, referred to as Isobut-5) was purchased from Dalian Date Gas Co., Ltd. Pinane (99 wt%) was purchased from McLean Reagent Co., Ltd. NH_4Cl (99 wt%, analytically pure) was purchased from Adamas.

Preparation of catalysts

The commercial zeolites ZSM-5, β-25n, β-25m, β-50m, ZSM-35, SAPO-11, and Y were subjected to a calcination process to remove any residual template or adsorbed substances, at a temperature of 550 °C for 3 h in static air. Following the calcination process, ion exchange was performed using a 1 mol L^{-1} NH_4Cl solution. The zeolites were immersed in the NH_4Cl solution at a ratio of 25 mL g^{-1} and the temperature was set at 80 °C. The mixture was agitated at a speed of 600 rpm for a duration of 3 h. After the ion exchange process, the solid was

separated through filtration and washed thoroughly, and then dried overnight at a temperature of 80 °C. Subsequently, the dried solid was ground into a powder form and subjected to a further calcination process at a heating rate of 2 °C min^{-1} to 550 °C. The calcination was carried out under static air for a duration of 3 h to obtain the H-type molecular sieve. In a separate step, HPW hydrate was also calcined in static air. The temperature was initially increased at a heating rate of 2 °C min^{-1} to 250 °C for 3 h to remove the crystal water in HPW.

Catalyst characterizations

X-ray fluorescence (XRF) spectrum was employed to analyze the actual molar ratio of silicon to aluminum in zeolites. The solid sample was directly tested using a RIGAKUZSX Priums spectrometer under vacuum conditions. The instrument model had an observation diameter of 26 mm, an observation area of 530.93 m^3, and a sample height of 25 mm. The desired error range for the analysis was within 0.01 to ensure accurate results.

Pyridine adsorption followed by Fourier transform infrared spectroscopy (FT-IR) was performed using a Nicolet6700 spectrometer with a transmission MCT/B detector. Before analysis, the sample was pressed into a self-supporting chip with a density of approximately 10 mg cm^{-2} and treated under vacuum at 450 °C for 4 h. Pyridine adsorption was conducted at 120 °C under a partial pressure of 3.5 torr for 20 min. After adsorption, the samples were subjected to desorption at 120, 180, and 250 °C, respectively. The intensity of acid sites was studied by recording FT-IR spectra at room temperature, with a resolution of 4 cm^{-1} and an accumulation of 128 scans for a single spectrum. The concentrations of Lewis and Brønsted acid sites in the zeolite were evaluated based on the band integral strength at 1454 cm^{-1} (C_{Lewis}) and 1545 cm^{-1} ($C_{Brønsted}$), respectively, as observed in the FT-IR spectra.

An ASAP2460 N_2 adsorption/desorption instrument was employed to determine the pore parameters of zeolites. Before conducting the test, the zeolite sample was subjected to high-temperature degassing at 300 °C in a degassing pipe to remove any excess water present in the molecular sieve's pore channels. The degassing condition involved maintaining a temperature of 300 °C for 4 h. After that, the zeolite sample was subjected to adsorption and desorption under the operating condition at −196 °C for 24 h. The specific surface area (S_{BET}) was evaluated using the BET method. The Barret Joyner Hallenda (BJH) method was utilized to determine the mesoporous volume (V_{meso}) from the isotherm curve. The total pore volume (V_{total}) was determined using the single-point method. The microporous volume (V_{micro}), microporous surface area (S_{micro}), and mesoporous surface area (S_{exter}-including surface area) were confirmed using the t-plot method.

The particle size of the β zeolite sample was determined using a Mastersizer 2000/3000 laser particle size analyzer. A suitable amount of zeolite powder was mixed with deionized water to prepare a suspension. After 20 min of ultrasonic dispersion, the measurement was conducted under constant temperature conditions at 25 °C.

Temperature-programmed desorption of ammonia (NH$_3$-TPD) was conducted using an AutoChemII2920 chemisorption analyzer. Before the measurement, approximately 0.1 g of dry sample was subjected to degassing in a flow of helium at 400 °C for 1 h. After cooling the sample to 100 °C, it was exposed to a flow of NH$_3$ (10% volume) mixed with helium for 30 min. And then the sample was purged with He gas for 1 h to remove any physically adsorbed NH$_3$. Subsequently, a temperature-programmed desorption ranged from 100 °C to 600 °C at a heating rate of 10 °C min^{-1}. The residual NH$_3$ desorbed during this process was quantitatively analyzed using a gas chromatograph LHM-80 equipped with a thermal conductivity detector. The resulting desorption curve was recorded as the ammonia temperature programmed desorption curve.

For the measurement of coke formed on the catalyst during the reaction, temperature-programmed oxidation (TPO) was performed using the AutoChemII2920 chemisorption analyzer. Initially, the sample (weighing between 0.015 g to 0.020 g) was treated in a flow of N$_2$ at reaction temperature for 30 min. Subsequently, it was heated from room temperature to 800 °C at a rate of 10 °C min^{-1}, using a flow of 2% O$_2$/N$_2$ mixture. At a temperature of 673 °C, the generated CO$_2$ was converted to methane using a methanation catalyst (Ni/silica–alumina), and detection was performed using a flame ionization detector in the SRI-8610C gas chromatograph.

Alkylation reaction process and products analysis method

A mixture containing 1 mL of α-pinene, 1 mL of pinane, and 0.1 g of catalyst was added into a stainless-steel high-pressure reactor with a polytetrafluoroethylene lining. The air inside the reactor was then purged three times using continuous charging and venting with nitrogen to remove any oxygen. Next, a volume of 4 mL of Isobut-5 was filled into the reactor with the double plunger trace pump. The reaction was conducted at the set temperature for 5 h with a stirring speed of 420 rpm. After that, the reactor was cooled down to room temperature, and the resulting liquid mixture was sampled for product analysis after centrifuging.

Qualitative analysis was conducted using Agilent 7890A/5975C gas chromatography-mass spectrometry (GC-MS) equipped with a DB-5 column (30 m × 0.32 mm × 0.25 μm). Quantitative analysis was carried out using gas chromatography (GC-9790, Fuli instrument) equipped with a DB-5 column (30 m × 0.32 mm × 0.25 μm). N$_2$ at 0.4 MPa was used as the carrier gas. The detector temperature and vaporization chamber temperature were both set to 280 °C. The temperature program was as follows: The temperature was ramped from 40 °C (kept for 1 min) at a rate of 5 °C min^{-1} until reaching 50 °C, and then increased at a rate of 10 °C min^{-1} to 160 °C and held for 1 min. Subsequently, the temperature was increased at a rate of 20 °C min^{-1} to a final temperature of 280 °C, with a hold time of 20 min.

Calculation

The compound's structure was geometrically optimized using DFT-B3LYP in the Gaussian09 package, employing the 6-311G(d,p) basis set to obtain a stable configuration. The volume of the molecule was determined through surface analysis using the Multiwfn 3.8 program. The optimization was conducted without any symmetry constraints, employing default convergence criteria. All modified structures were located at the minimum energy point on the potential energy surface and did not exhibit any imaginary frequencies.[27]

Results and discussion

Analysis of products in the system of α-pinene alkylation with Isobut-5

The reaction between α-pinene and isobutene/isobutane is commonly recognized as a typical carbonium ion reaction.[12,28] The typical product distribution over HPW analyzed by GC is shown in Fig. 1. Combined with GC-MS analysis (Fig. S1, ESI†), the main processes involved in the reaction system are illustrated in Scheme 1. These include: monomolecular isomerization of α-pinene (R1, R2) to generate camphene, limonene, and other isomers; cross-alkylation of α-pinene (or its isomers) with isobutene (R3, R4, R5) to produce C$_{14}$ products; cross-alkylation between α-pinene and its isomers (R6, R7, R8) resulting in the formation of dimers; self-alkylation of isobutene and isobutane (R10) leading to the generation of C$_8$ components; a small amount of C$_8$ components further undergoes alkylation (R11), resulting in the production of C$_{12}$, C$_{16}$, and other products; and dehydrogenation of limonene (or other ring-opening isomers of α-pinene) (R9) yielding p-cymene.

According to the analysis conducted using Gaussian 09 and Multiwfn 3.8 programs, based on DFT-B3LYP and 6-311G** calculations, the optimized structures and dimensions of typical molecules in this reaction system are presented in Table S1 (ESI†). It can be observed that the products obtained from α-pinene isomerization exhibit slightly smaller molecular dimensions compared to α-pinene itself. Conversely, the products formed through bimolecular alkylation reactions have larger sizes, with C$_{14}$ products ranging from 0.61 to 0.63 nm,
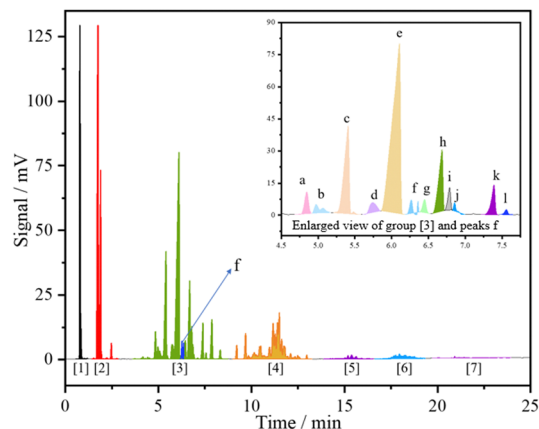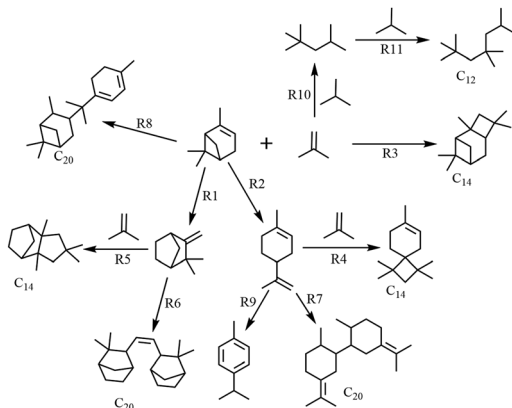

Fig. 1 Typical alkylation products distribution of α-pinene and Isobut-5 measured by GC. [1] C$_4$; [2] C$_8$; [3] C$_{10}$; [4] C$_{14}$; [5] C$_{15}$–C$_{20}$; [6] C$_{20}$; [7] oligomers; (a) tricyclene; (b) α-pinene; (c) camphene; (d) β-pinene; l pinane; (f) C$_{12}$; (g) α-terpinene; (h) p-cymene; (i) limonene; (j) menthene; (k) γ-terpinene; (l) terpinolene.

Scheme 1 Possible alkylation route of α-pinene and Isobut-5.[13,19–21]

and C_{20} products ranging from 0.69 to 0.73 nm. The oligomers of α-pinene are expected to have even larger molecular sizes.[27] Therefore, the pore structure of molecular sieves is believed to play a critical role in influencing the reaction when zeolite catalysts are employed.[24,26,29]

Catalytic performance of various zeolites for α-pinene alkylation with Isobut-5

The catalytic results of Hβ-25n, HY, HZSM-5, HZSM-35, and HSAPO-11 in the reaction between α-pinene and Isobut-5 are presented in Fig. 2. The results of NH_3-TPD and Py-IR in Fig. 3 (also see Table S2, ESI†) reveal that the catalytic performance of these zeolites does not show a clear correlation with their acid distribution.

In Fig. 3a, it can be observed that HSAPO-11, in addition to weak acid sites, exhibits a peak of medium-strength acid sites at 300 °C, while Hβ-25n, HZSM-5, and HZSM-35 have peaks of strong acid sites at 400 °C. However, no significant desorption peaks above medium-strength acids are observed in the desorption curves of HY. According to the data in Table S2 (ESI†), HY exhibits the highest total acid amount among the various zeolites, followed by HZSM-5. Fig. 3b demonstrates that the acid sites of HY and HSAPO-11 are predominantly Lewis acids, which is related to their lower Si/Al ratios. HZSM-5 and HZSM-35, on the other hand, primarily possess Brønsted acid sites. Hβ-25n zeolite exhibited a relatively stable distribution of both Brønsted and Lewis acid sites across all acid strengths. As shown in Fig. 2a, the conversion of α-pinene gradually increased with the rising reaction temperature for all zeolite catalysts after a reaction time of 5 h. However, at temperatures below 140 °C, HZSM-5, HZSM-35, and HSAPO-11, which have strong or medium-strength acid sites, can hardly catalyze the conversion of α-pinene. This can be attributed to their small microporous structures (5.3 × 5.6 10MR, 4.2 × 5.4 10MR, and 4.0 × 6.5 10MR) (database of zeolite structures), which inhibit the diffusion of α-pinene (0.58 nm) and the occurrence of its bimolecular reactions. Consequently, only partial monomolecular isomerization of α-pinene occurs on the external surface of the zeolites at the higher reaction temperature, as shown in Fig. 2c. Additionally, Fig. 2a indicates that Hβ-25n can achieve

an α-pinene conversion comparable to that of HPW when the reaction temperature reaches 120 °C, while the activity of HY, despite having the highest total acid amount, is not as satisfactory. These findings suggest that the pore structure of the zeolite molecular sieve plays a more significant role in catalyzing this reaction than its acid properties.

The nitrogen adsorption–desorption results (Fig. 4 and Table S3, ESI†) reveal that HY, HZSM-5, and HZSM-35 exhibit typical characteristics of microporous structures with pore sizes of approximately 0.75 nm, 0.5 nm, and 0.55 nm, respectively. This explains why these zeolites show lower catalytic activity for α-pinene conversion in Fig. 2a, regardless of their acid strength or acid amounts. On the other hand, HSAPO-11, with its one-dimensional structure, has fewer micropores and a lower surface area. Its limited pore volume is primarily distributed in mesopores around 1.5 nm, which, combined with the weaker acidity, results in weaker catalytic performance. In contrast, Hβ-25n exhibits a hysteresis loop at $P/P_0 = 0.4$ in Fig. 4a, indicating the presence of mesopores in addition to micropores. Fig. 4b demonstrates that the micropores of Hβ-25n are mainly distributed between 0.6–0.7 nm, and the mesopores are primarily distributed between 2–4 nm. These larger pores provide sufficient space for the diffusion of α-pinene, facilitating its adsorption and activation by the acidic active sites, thereby enabling the bimolecular alkylation reaction described in Scheme 1.

The observed results in Fig. 2b–e are consistent with the characterization findings mentioned earlier. HZSM-5, HZSM-35, and HSAPO-11 show difficulties in catalyzing the bimolecular reaction to form C_8, C_{14}, and C_{20} products, but they can catalyze the monomolecular isomerization of α-pinene at higher reaction temperatures. Furthermore, the selectivity of α-pinene isomers over HPW, Hβ-25n, and HY reaches its maximum at 100 °C, 110 °C, and 120 °C, respectively, indicating that higher reaction temperatures facilitate the further cross-alkylation of these isomers to generate C_{14} or C_{20} products. In addition, under the catalysis of HPW, which possesses strong Brønsted acidity and lacks diffusion limitations, higher production of C_8 products was observed, along with the detection of undesired oligomers in the liquid product mixture. In contrast, the content of C_8, C_{14}, and C_{20} products catalyzed by Hβ-25n all increased with increasing reaction temperature.

Fig. 2f also examines the catalytic activity and product distribution of Hβ-25n, HZSM-5, and HY in the self-alkylation of Isobut-5 (under the conditions of 4 mL Isobut-5, 0.1 g catalyst, 120 °C, and 5 h). It is observed that not only Hβ-25n and HY exhibit catalytic activity of self-alkylation, but the pore size of HZSM-5 is also sufficient to allow the C_4 hydrocarbons to enter the micropores and undergo self-alkylation. Additionally, the catalytic activity is correlated with the acidity of the zeolite. The zeolites with higher concentrations of strong acid sites facilitate consecutive reactions, resulting in a higher selectivity towards C_{12} products. By combining the results from Fig. 2a–e, it can be deduced that there is competitive adsorption between α-pinene and isobutene on the acid sites, with α-pinene showing a preference for adsorption.
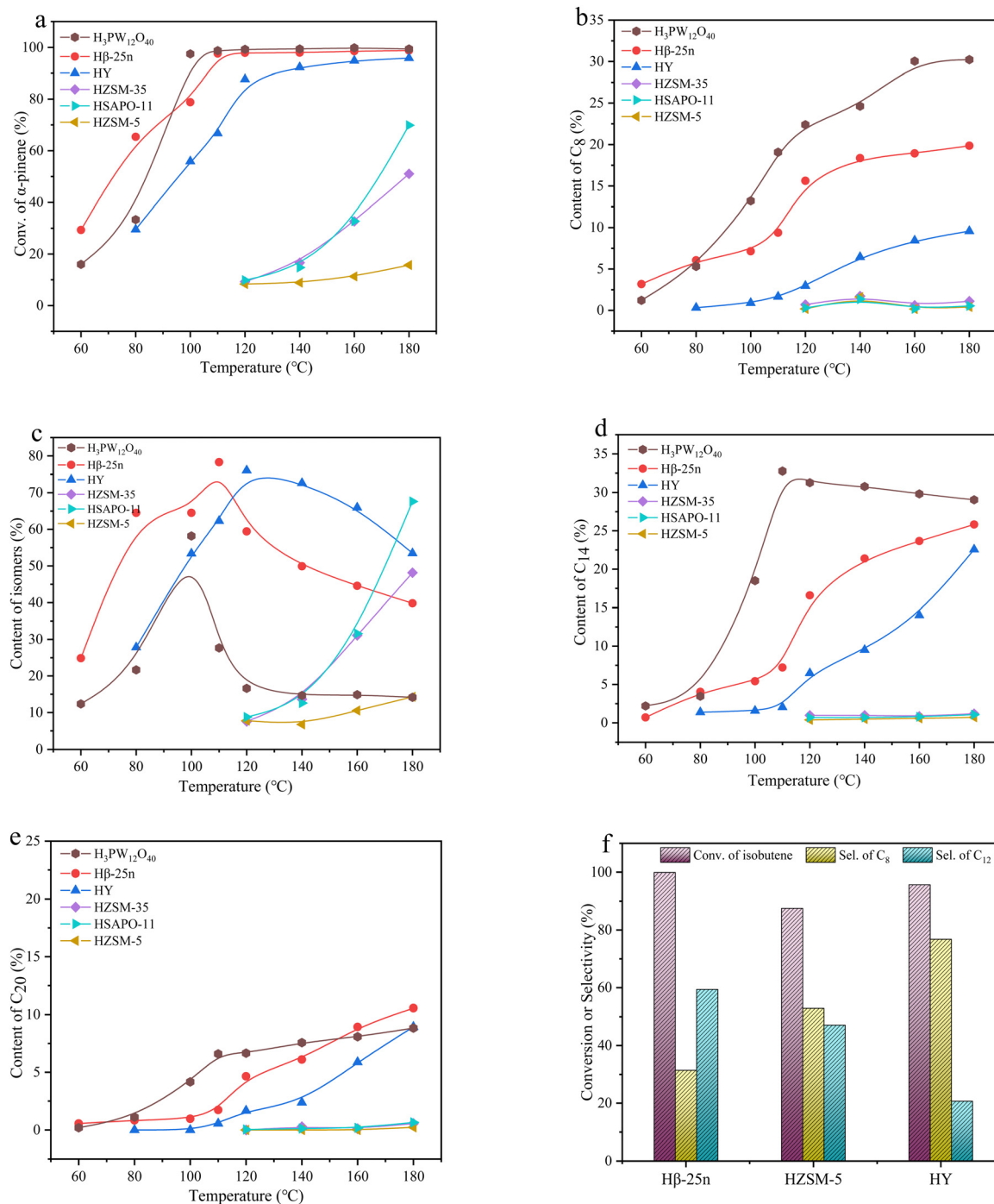
Fig. 2 (a)–(e) Conversion of α-pinene and products distribution catalyzed by various zeolites; (f) self-alkylation of Isobut-5 over Hβ-25n, HZSM-5, and HY. Reaction conditions: $V_{Isobut-5} : V_{α-pinene} : V_{pinane} = 4 : 1 : 1$, 0.1 g catalyst per $mL_{α-pinene}$, 5 h.

Influence of particle size and Si/Al ratio of β zeolite on the catalytic alkylation

A comparison of Hβ-25n, Hβ-25m, and Hβ-50m, with different particle morphologies and Si/Al ratios, was conducted to further investigate the impact of the zeolite pore structure and acid distribution of zeolites on the alkylation of α-pinene with Isobut-5. As depicted in Fig. 5, the order of activity for the three β-zeolites was Hβ-25n > Hβ-25m > Hβ-50m at lower reaction temperatures.

However, when the temperature was higher than 140 °C, the conversion of α-pinene for all three β zeolites approached 99%. Furthermore, the production of bimolecular alkylation products, such as C_8, C_{14}, and C_{20}, was all the highest under the catalysis of Hβ-25n, indicating that the influence of particle morphology on products distribution is more significant than that of Si/Al ratios.

From Fig. 6a, b and Table S4 (ESI†), it can be observed that Hβ-25n, Hβ-25m, and Hβ-50m exhibit similar pore structures,
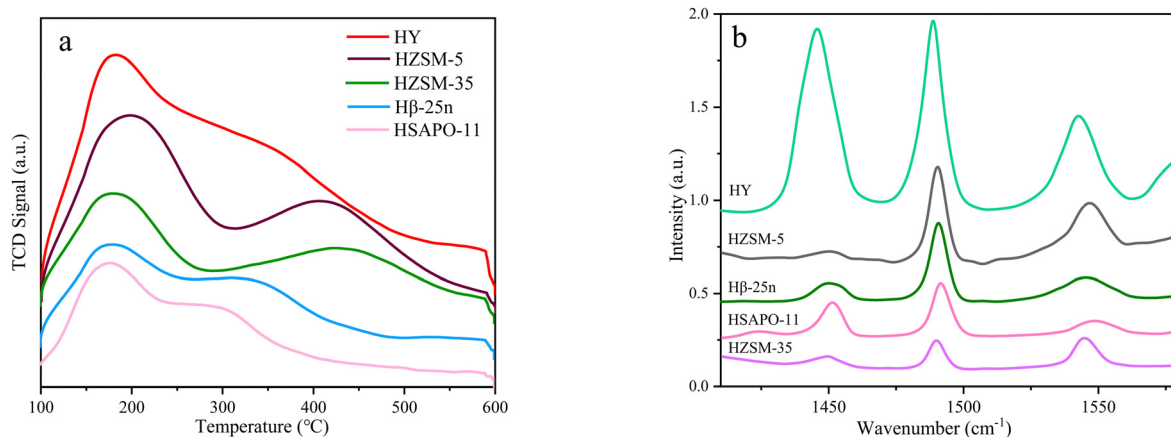
Fig. 3 Acid distribution of various zeolites (a) NH₃-TPD profiles; (b) Py-IR profiles.

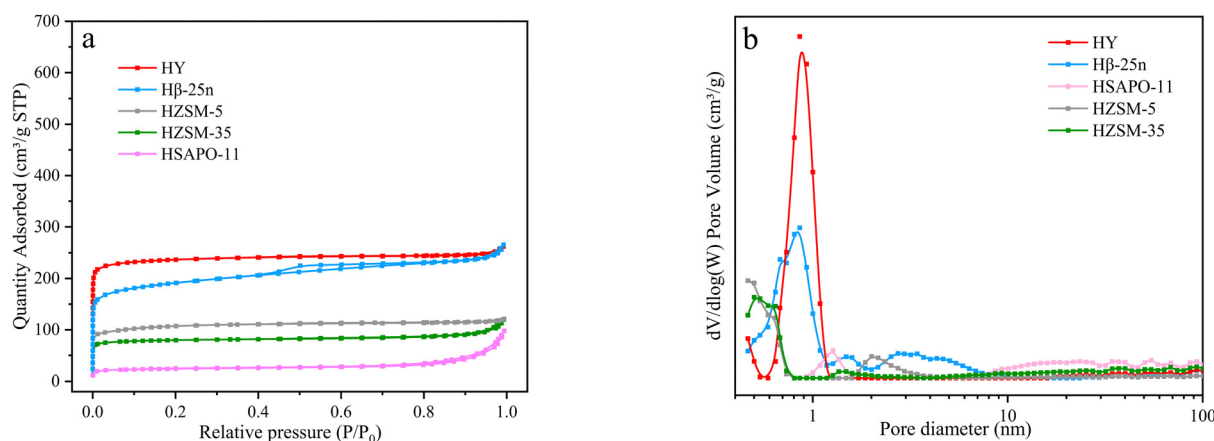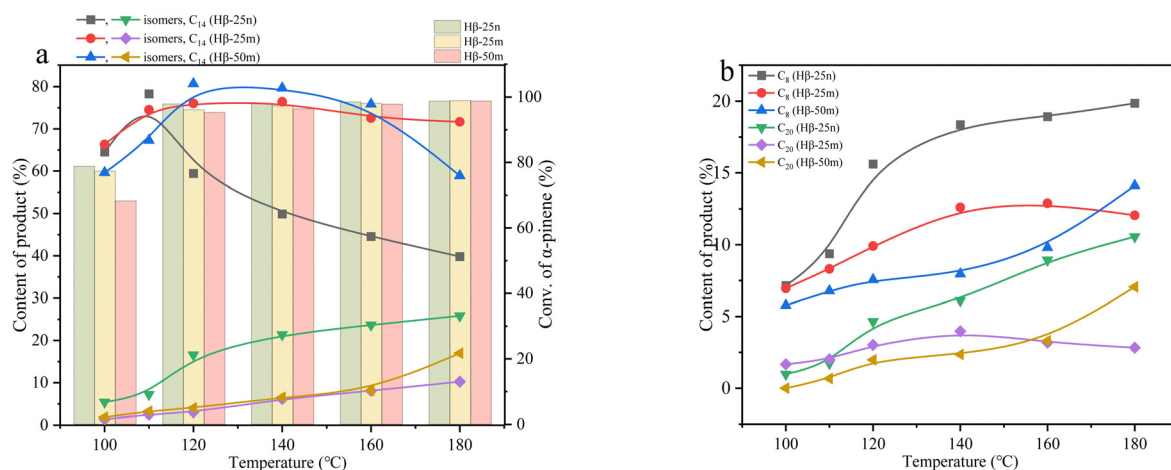Fig. 4 (a) N₂ adsorption/desorption isotherms and (b) pore size distribution of various zeolites.

Fig. 5 Alkylation performance of α-pinene with Isobut-5 over various Hβ zeolites: (a) conversion of α-pinene and content of isomers and C₁₄; (b) content of C₈ and C₂₀. Reaction conditions: V_Isobut-5 : V_α-pinene : V_pinane = 4 : 1 : 1, 0.1 g catalyst per mL_α-pinene, 5 h.

micropore volumes, and micropore specific surface areas. However, Hβ-25n shows a smaller particle size compared to Hβ-25m and Hβ-50m. In addition, it exhibits the largest

disparity between the volume surface diameter (D(4,3)) and the area surface average diameter (D(3,2)). This discrepancy implies that a considerable proportion of shorter nanoscale

microporous pores are present in the Hβ-25n zeolite particles, which provide a more favorable environment for the diffusion of reactants and products. Moreover, Hβ-25n zeolite also displays more mesopores around 1.5 nm and 3 nm, leading to markedly increased external specific surface area when compared to Hβ-25m and Hβ-50m. This expanded surface area provides a more suitable reaction space for the bimolecular reactions of α-pinene. The results from NH₃-TPD and FT-IR in Fig. 6c and d (also see Table S5, ESI†) demonstrate that Hβ-25n exhibits higher acid strength and a higher concentration of acid sites in comparison to Hβ-25m and Hβ-50m, with Brønsted acid sites being the predominant type. This confirms the influence of acid strength, acid concentration, and acid site type on the reaction performance.

Product distribution with reaction time over Hβ-25n

Fig. 7a and b depicts the variations in the conversion of α-pinene and the selectivity of resulting C_8 products at different reaction times using Hβ-25n and HPW catalysts, respectively. It is evident that the strong acidity of the HPW catalyst leads to a rapid increase in the conversion of α-pinene within a short duration, indicating its significantly superior catalytic activity compared to Hβ-25n. However, the selectivity of C_8 products over HPW is also considerably higher than that over Hβ-25n. Nevertheless, as the reaction time prolongs, the selectivity of C_8 products over Hβ-25n also shows a continuous increase.

Furthermore, Fig. 7c reveals that the initial stage of the reaction catalyzed by Hβ-25n primarily involves the isomerization of α-pinene. Among the resulting isomerization products, camphene and limonene are the most abundant. The selectivity of isomers reaches its peak after approximately 1 h of reaction time, followed by a sharp decline. Meanwhile, the selectivity of cross-alkylation products, namely C_{14} and C_{20}, exhibits a distinct increase. This suggests that the C_{14} and C_{20} products obtained under the catalysis of Hβ-25n mainly arise from the bimolecular alkylation of the α-pinene isomers, such as camphene and limonene. These C_{14} and C_{20} components, which possess favorable fuel properties, increase in selectivity as the reaction time progresses. However, at the same time, the C_8 component also increases. At 5 h of reaction time, the selectivity of C_8, C_{14}, and C_{20} are 14.1%, 27.0%, and 7.0%, while at 7 h, the selectivity of C_8, C_{14}, and C_{20} are 15.6%, 30.0%, and 7.8%, respectively.

Recycling performance of Hβ-25n in the alkylation of α-pinene with Isobut-5

After completing a run of catalytic reaction, the Hβ-25n catalyst was separated from the liquid mixture through centrifugation, washed with anhydrous ethanol, and dried. Subsequently, the catalyst was subjected to calcination at 500 °C for 3 h in preparation for the next run. The catalytic performance of the reused Hβ-25n was evaluated in each cycle, and the results are
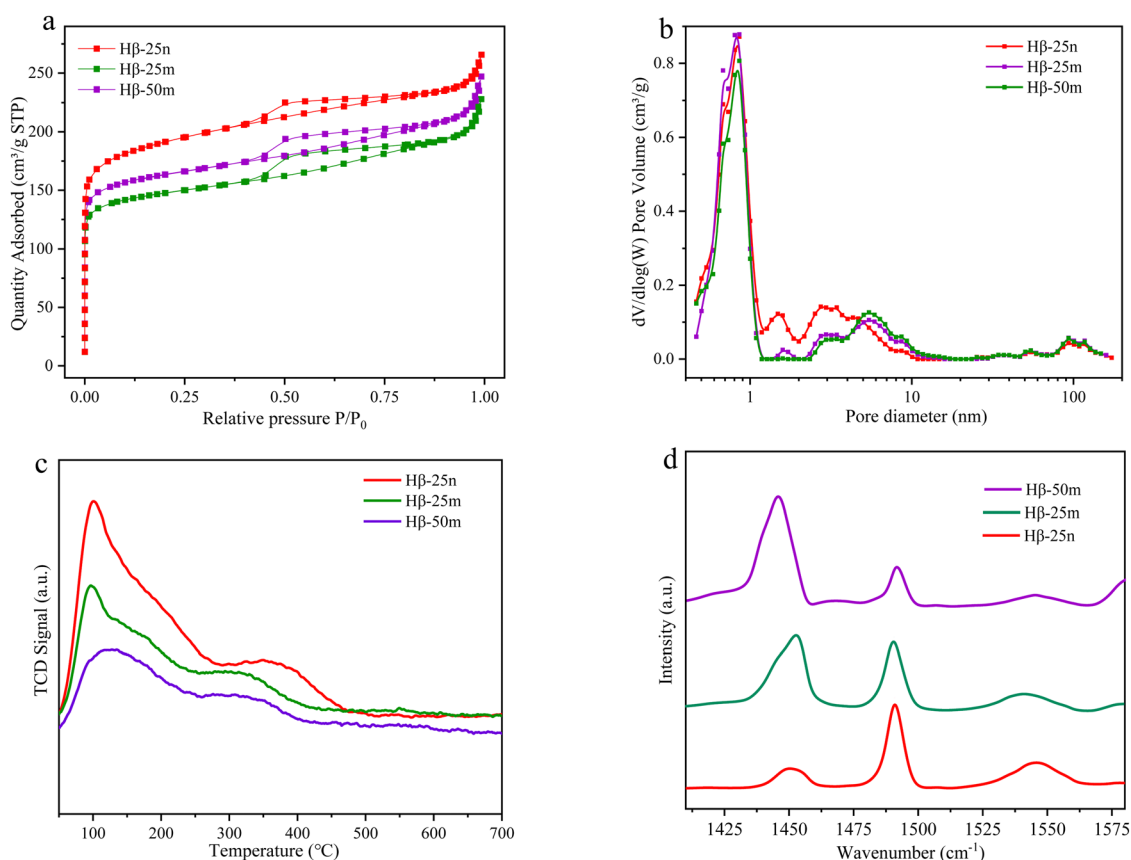

Fig. 6 (a) N₂ adsorption–desorption curves; (b) pore size distribution; (c) NH₃-TPD adsorption curves; (d) Py-IR curves of β zeolites.
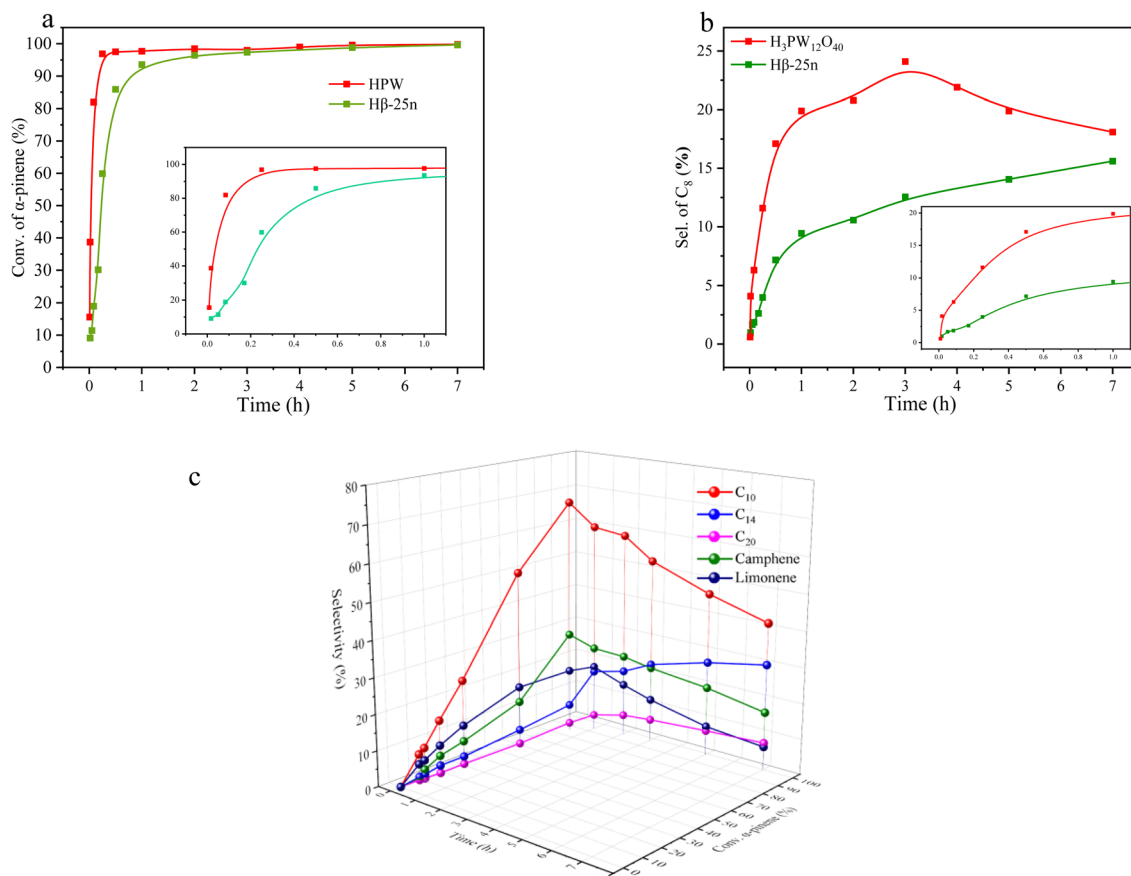
Fig. 7 Alkylation performance over Hβ-25n with different reaction time: (a) α-pinene conversion; (b) C$_8$ selectivity; (c) distribution of various typical products. Reaction conditions: V$_{Isobut-5}$: V$_{α-pinene}$: V$_{pinane}$ = 4 : 1 : 1, 0.1 g catalyst per mL$_{α-pinene}$, 120 °C.

presented in Fig. 8a. It can be observed that Hβ-25n maintained a high α-pinene conversion of approximately 98% during the first three runs. However, the selectivity for C$_{14}$ components gradually decreased. Particularly, the conversion of α-pinene dropped to 71.1%, while the selectivity for C$_{14}$ decreased to 7.1% in the fourth run. This decline in performance can be attributed to the blockage of the pores and active sites by

carbon deposits on the catalyst surface. Additionally, as the catalyst was repeatedly used, the formation of α-pinene oligomers became evident in the products (Fig. S2, ESI†). This phenomenon is also linked to the hindered diffusion resulting from carbon deposition, which triggers a series of consecutive reactions. The temperature-programmed oxidation (TPO) curve depicted in Fig. 8b confirms the presence of two types of carbon
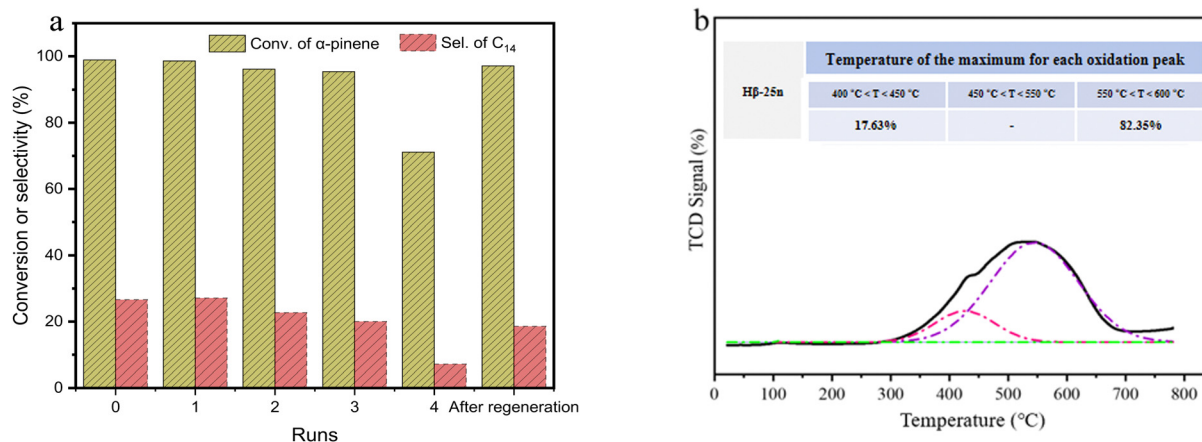

Fig. 8 Recycling performance of Hβ-25n catalysts: (a) conversion of α-pinene and selectivity of C$_{14}$; (b) TPO curves of Hβ-25n after 4 runs. Reaction conditions: V$_{Isobut-5}$: V$_{α-pinene}$: V$_{pinane}$ = 4 : 1 : 1, 0.1 g catalyst per mL$_{α-pinene}$, 5 h, 120 °C.

deposits on the Hβ-25n zeolite surface after four runs of catalysis. Approximately 17.65% of the carbon deposits can be oxidized within the temperature range of 400 to 450 °C, while the remaining 82.35% necessitate oxidation temperatures between 550 and 600 °C.

To address the decline in catalytic activity, the spent Hβ-25n catalyst underwent regeneration *via* calcination at 600 °C for 3 h. As illustrated in Fig. 8a and Fig. S2 (ESI†), the regenerated catalyst exhibited a significant recovery in both conversion and selectivity for C_{14} components. Notably, the formation of oligomer byproducts was no longer observed. This finding further supports the notion that carbon deposition is the primary cause of the decrease in the catalytic activity of Hβ-25n zeolite and can be effectively remedied through regeneration under the specified calcination conditions at 600 °C.

Conclusions

This study analyzed and calculated the sizes of various typical compounds in the α-pinene and Isobut-5 (isobutene/isobutane mixture) alkylation reaction system. The catalytic performance of different zeolites, including Hβ, HY, HZSM-35, HZSM-5, and HSAPO-11, in this reaction was investigated. Through analysis and characterization of their pore size, pore structure, and acidity, it was confirmed that the nano-sized Hβ-25n zeolite with its suitable meso-microporous structure and acidity facilitates the adsorption of α-pinene and subsequent reactions. The shorter pore channels of Hβ-25n also provide favorable conditions for the diffusion of reactants and the bimolecular alkylation products. The study on the cyclic performance of Hβ-25n revealed that only a portion of carbon deposits can be removed by calcination at 500 °C, while the majority of carbon deposits can be eliminated at around 600 °C. The regeneration of Hβ-25n at 600 °C effectively prevents the decline in activity and the formation of oligomer byproducts caused by pore blockage and coverage of active sites, thus restoring the catalytic activity of Hβ-25n zeolite.

Data availability

The authors confirm that the data supporting the findings of this study are available within the article and its ESI.†

Author contributions

Zhaocai Jiao: investigation, data curation, validation, visualization. Mingzu Liu: data curation, formal analysis, investigation, writing – original draft. Ningbo Yang: investigation. Fengli Yu: resources. Congxia Xie: resources, funding acquisition. Shitao Yu: Resources, Supervision. Bing Yuan: conceptualization, formal analysis, supervision, writing – review & editing, resources, funding acquisition.

Conflicts of interest

There are no conflicts to declare.

Acknowledgements

References

1 R. Batten, M. Karanjikar and S. Spatari, *Sustainable Energy Fuels*, 2024, **8**, 1924–1935.
2 J. Carvalho, A. Vieira, A. Magalhães, L. S. M. Miranda, Y. L. Lam and M. M. Pereira, *Sustainable Energy Fuels*, 2024, **8**, 1329–1337.
3 G. Shrivastav, T. S. Khan, M. Agarwal and M. A. Haider, *ACS Sustainable Chem. Eng.*, 2017, **5**, 7118–7127.
4 W. Xu, K. Mou, H. Zhou, J. Xu and Q. Wu, *Green Chem.*, 2022, **24**, 6589–6598.
5 C. Yu, S. Yu and L. Li, *Fuel*, 2022, **308**, 122038.
6 S. Tang, X. Duan, Q. Zhang, C. Wang, W. Wang, W. Feng and T. Wang, *Biomass Convers. Biorefin.*, 2024, **14**, 2311–2320.
7 S. Huang, X. Luo, J. Li, S. Liu and L. Shuai, *Green Chem.*, 2024, **26**, 4043–4050.
8 J. Bai, Y. Zhang, X. Zhang, C. Wang and L. Ma, *ACS Sustainable Chem. Eng.*, 2021, **9**, 7112–7119.
9 L. R. Lynd, G. T. Beckham, A. M. Guss, L. N. Jayakody, E. M. Karp, C. Maranas, R. L. McCormick, D. Amador-Noguez, Y. J. Bomble, B. H. Davison, C. Foster, M. E. Himmel, E. K. Holwerda, M. S. Laser, C. Y. Ng, D. G. Olson, Y. Román-Leshkov, C. T. Trinh, G. A. Tuskan, V. Upadhayay, D. R. Vardon, L. Wang and C. E. Wyman, *Energy Environ. Sci.*, 2022, **15**, 938–990.
10 W. Wang, N. Li, G. Li, S. Li, W. Wang, A. Wang, Y. Cong, X. Wang and T. Zhang, *ACS Sustainable Chem. Eng.*, 2017, **5**, 1812–1817.
11 X. Luo, R. Lu, X. Si, H. Jiang, Q. Shi, H. Ma, C. Zhang, J. Xu and F. Lu, *J. Energy Chem.*, 2022, **69**, 231–236.
12 B. Yuan, Z. Wang, X. Yue, F. Yu, C. Xie and S. Yu, *Renewable Energy*, 2018, **123**, 218–226.
13 B. G. Harvey, M. E. Wright and R. L. Quintana, *Energy Fuels*, 2010, **24**, 267–273.
14 J. M. Winter and Y. Tang, *Curr. Opin. Biotechnol*, 2012, **23**, 736–743.
15 A. Kern, E. Tilley, I. S. Hunter, M. Legiša and A. Glieder, *J. Biotechnol.*, 2007, **129**, 6–29.
16 J. Zhu, J. V. Alegre-Requena, P. Cherry, D. Curtis, B. G. Harvey, M. A. Jabed, S. Kim, C. S. McEnally, L. D. Pfefferle and J.-D. Woodroffe, *Proc. Combust. Inst.*, 2023, **39**, 877–887.
17 J. K. Jung, Y. Lee, J.-W. Choi, J. Jae, J.-M. Ha, D. J. Suh, J. Choi and K.-Y. Lee, *Energy Convers. Manage.*, 2016, **116**, 72–79.

18 Y. Liu, C. Shi, L. Pan, X. Zhang and J.-J. Zou, *Fuel*, 2022, **307**, 121906.

19 F.-L. Yu, G.-X. Li, Y.-L. Gu, C.-X. Xie, B. Yuan and S.-T. Yu, *Catal. Today*, 2018, **310**, 141–145.

20 M. Liu, X. Zhao, Z. Ma, B. Yuan, F. Yu, C. Xie and S. Yu, *Chem. Eng. Sci.*, 2023, **281**, 119174.

21 G. Nie, J.-J. Zou, R. Feng, X. Zhang and L. Wang, *Catal. Today*, 2014, **234**, 271–277.

22 M. J. Janik, R. J. Davis and M. Neurock, *J. Catal.*, 2006, **244**, 65–77.

23 Y. Wang, J. Liu, Z. Zhao, Q. Guo, Q. Jiang, N. He and F. Wang, *Appl. Catal., B*, 2022, **307**, 121139.

24 D. Parmar, S. H. Cha, T. Salavati-fard, A. Agarwal, H. Chiang, S. M. Washburn, J. C. Palmer, L. C. Grabow and J. D. Rimer, *J. Am. Chem. Soc.*, 2022, **144**, 7861–7870.

25 M. K. Montañez Valencia, C. L. Padró and M. E. Sad, *Appl. Catal., B*, 2020, **278**, 119317.

26 J. Wu, S. Wang, H. Li, Y. Zhang, R. Shi and Y. Zhao, *Nanomaterials*, 2019, **9**, 1192.

27 B. Zhu, X. Zhao, Y. Zhang, B. Yuan, F. Yu, C. Xie and S. Yu, *Biomass Bioenergy*, 2023, **174**, 106859.

28 M. Jin, M. Oh and M. Choi, *ACS Catal.*, 2022, **12**, 4067–4077.

29 Database of Zeolite Structures, **https://asia.iza-structure.org/IZA-SC/ftc_table.php**.